Int. J. Heat Mass Transfer. Vol. 30, No. 6, pp. 1133–1148, 1987
Printed in Great Britain

0017-9310/87 $3.00 + 0.00
© 1987 Pergamon Journals Ltd.

Condensation heat transfer studies for stratified, cocurrent two-phase flow in horizontal tubes

I. Y. CHEN† and G. KOCAMUSTAFAOGULLARI
Department of Mechanical Engineering, University of Wisconsin—Milwaukee, Milwaukee, WI 53201, U.S.A.

(*Received* 13 *February* 1986 *and in final form* 21 *October* 1986)

Abstract—Condensation heat transfer inside horizontal tubes is investigated for a stratified, cocurrent two-phase flow of vapor and liquid. The analysis takes into account the effects of interfacial shear, axial pressure gradient, saturation temperature level, driving temperature difference and the development of the stratified angle associated with the accumulated condensate layer at the bottom of the tube. The influence of these parameters is evaluated with respect to the peripheral condensate film heat transfer performance for the practically interesting laminar flow range of operating conditions of water-vapor flow. A theoretical predictive method is developed to obtain the overall heat transfer coefficient along the tube length. Results of the theoretical predictions are found to agree favorably with the reported experimental data which cover a variety of fluids with a relatively wide range of operating conditions. A simple, predictive heat transfer coefficient correlation is proposed from the numerical solution by means of regression analysis.

1. INTRODUCTION

CONDENSATION inside a horizontal tube is common to many heat transfer devices and is particularly important in the chemical processes and power industries. The recent developments in horizontal tube evaporators, where filmwise condensation takes place inside horizontal tubes while the evaporating film flows over the outside of the tubes, have renewed interest in the film flow heat transfer problems associated with interfacial phase change. A complete analysis of a horizontal tube evaporator requires development of reliable predictive methods which can be used to evaluate the heat transfer coefficients of condensing and evaporating liquid films within the operating range of these evaporators. The investigation of condensation heat transfer of such a horizontal evaporator is the aim of this study.

Considering the actual operating range of vapor feeding into a horizontal tube evaporator, the vapor–condensate flow inside the tube is normally encountered as a stratified two-phase flow pattern [1–3]. Under the stratified-smooth or stratified-wavy flow patterns, it may be assumed that thin film condensation takes place at the upper portion of the tube and drains down while the condensate stratified layer flows along the bottom of the tube. As noted by Moalem and Sideman [4, 5], at relatively high vapor flow rates within the operating range of horizontal tube evaporators, the assumption of zero interfacial shear exerted by the vapor flow is not valid, although a stratified two-phase flow pattern still prevails. This indicates that any condensation heat transfer analysis inside horizontal tubes should include the effect of interfacial shear on the condensate film flow along the perimeter of the tube as well as on the condensate layer flow at the bottom of the tube.

Nusselt [6] was the first to analyze laminar film condensation on the outside of a horizontal tube. Chaddock [7] and Chato [8] applied Nusselt analysis to the problem of condensation in inclined horizontal tubes. They showed the effect of the liquid accumulating inside the tubes at low mass flow rates. Rufer and Kezios [9] included momentum effects on the stratified liquid flow and extended these studies to higher vapor flow rates. Jaster and Kosky [10] also derived an equation which predicts the rate of heat transfer in terms of void fraction and the Nusselt type heat transfer solutions. However, the effect of interfacial vapor shear is neglected in all of the above results.

Alternatively, numerous empirical heat transfer correlations have been developed from experimental observations [11–16]. Liquid Prandtl number, superficial Reynolds numbers of vapor, and liquid flow are commonly used as dimensionless groups to correlate data. Generally, the application of the proposed correlations is limited to their imposed geometric and predetermined experimental conditions. Therefore, marked disagreements may be observed if one correlation is applied to other data.

Although the effect of the interfacial shear on the stratified two-phase flow pattern has been extensively studied with respect to pressure drop and gas holdup [17–20], very little has been done analytically for the heat transfer and phase change aspects associated with the interfacial vapor shear acting on the condensate film flow draining down and on the stratified condensate flow. This may be partly due to the fact that analysis is quite difficult because the condensate film at the upper portion of the tube undergoes a

† Present address: Sundstrand Advanced Technology Group, Rockford, IL 61125, U.S.A.

NOMENCLATURE

A	cross-sectional area
A_g	vapor cross-sectional area
C_p	specific heat at constant pressure
d	diameter
d_h	hydraulic diameter
Fr	Froude number
f_i	interfacial friction factor
h_i	heat transfer coefficient based on inlet temperature
h_c	heat transfer coefficient for condensate film
h_l	heat transfer coefficient for accumulated condensate layer
h	overall heat transfer coefficient
h_{fg}	latent heat of condensation
j_f	superficial volumetric flux for liquid
j_{fl}	superficial volumetric flux for condensate layer
j_g	superficial volumetric flux for vapor
Ku	Kutateladze number
k	liquid conduction heat transfer coefficient
l	pipe length
$\dot{m}$	mass flow rate
$\dot{m}'$	mass flow rate per unit length
$\dot{m}''$	mass flow rate per unit area
Nu	Nusselt number
P	pressure
Pr	Prandtl number
q''	heat flux
Re	Reynolds number
Re_{ls}	superficial Reynolds number for liquid phase
Re_{gs}	superficial Reynolds number for vapor phase
T	temperature
T_s	saturation temperature
T_w	wall temperature
ΔT	temperature difference ($\equiv T_s - T_w$)
u, v, w	velocity components in x-, y- and z-directions, respectively
x	tangential coordinate for condensate film flow
y	radial coordinate for condensate film flow
z	axial coordinate.

Greek symbols

α	vapor void fraction
δ	film thickness
ξ	perimeter
μ	dynamic viscosity
ρ	mass density
τ	viscous shear
Φ	two-phase frictional pressure drop multiplier
ϕ	peripheral angle
ϕ_m	peripheral angle of condensate layer.

Subscripts

c	condensate film
f	liquid
g	vapor
i	tube inlet value
l	condensate layer.

three-dimensional motion under the simultaneous action of gravity and interfacial shear. Butterworth [21] and Moalem and Sideman [5] recognized the effect of interfacial shear on the condensation processes heat transfer coefficient inside a horizontal tube. They developed models which can be used to predict the heat transfer coefficient associated with condensation. Although the methods developed in refs. [5, 21] represent positive steps toward obtaining analytical solutions incorporating the effect of interfacial shear, it should be noted here that both studies included the axial shear effect in the formulation of the condensate layer only. As demonstrated by Chen [22] the axial shear and pressure gradient should also be included in formulating the circumferential condensate film flow.

In view of the above discussions, this paper has three objectives: (1) to develop a physical model which includes the effects of vapor flow, varying interfacial shear and pressure gradient to predict the condensation heat transfer coefficient for vapor–condensate flow in a horizontal tube; (2) to develop a numerical scheme to calculate the local and average heat transfer coefficients as well as to show effects of various parameters on heat transfer coefficients; and (3) based on numerical evaluations to develop a simple predictive correlation for the averaged heat transfer coefficient which can be used for practical purposes.

2. ANALYSIS

2.1. *Physical model*

The physical system is illustrated in Fig. 1. The present analysis considers a horizontal tube with an inside diameter d, and a length l, with a constant inside wall temperature, T_w. Saturated vapor at T_{si} ($T_{si} > T_w$) enters the horizontal tube at $z = 0$, and flows in the z-direction while it condenses on the surface of the tube. It is assumed that the vapor is at the local saturation temperature, $T_s = T_s(z)$. The condensate film flows tangentially, in the x-direction,

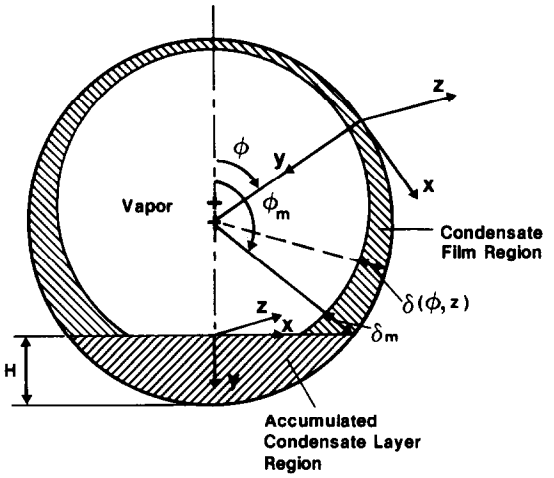

FIG. 1. Physical model and coordinates for condensate film flow and accumulated condensate layer flow for vapor condensation inside horizontal tubes under stratified conditions.

along the tube periphery under the influence of gravity whereas it is dragged in the axial direction by the interfacial vapor shear. Contrary to the existing condensation analyses of horizontal pipes, the condensate film flow in the upper portion of a pipe is not assumed to be entirely circumferential. In addition to the axial vapor flow and the liquid film flow described here, the accumulated condensate at the bottom of the tube flows axially, in the z-direction, under the influence of interfacial shear. The hydrodynamics of these three distinctive flow fields, i.e. condensate film flow, accumulated condensate flow, and vapor flow, determine the heat-transfer mechanism; and, therefore, simultaneous solutions of the field equations are desirable in order to obtain heat transfer predictions.

2.2. *Condensate film flow*, $0 \leq \phi \leq \phi_m$

It is assumed that the condensate film flow is laminar and that the thickness of the condensate film is small compared to the tube diameter, and the curvature effect is neglected. The field equations governing the kinematic, dynamic and energetic fields of the flow are simplified by using the thin film approximation. A detailed consideration of the relative order of magnitude of the various dimensionless parameters, justification for neglecting various terms, and discussion of appropriate scaling were given by Chen [22].

The simplified governing equations are given as follows:

continuity equation

$$\frac{\partial u}{\partial x} + \frac{\partial v}{\partial y} + \frac{\partial w}{\partial z} = 0 \tag{1}$$

x-component of momentum equation

$$\mu \frac{\partial^2 u}{\partial y^2} + \Delta\rho g \sin\phi = 0 \tag{2}$$

z-component of momentum equation

$$\mu \frac{\partial^2 w}{\partial y^2} - \frac{\mathrm{d}P}{\mathrm{d}z} = 0 \tag{3}$$

energy equation

$$\frac{\partial^2 T}{\partial y^2} = 0. \tag{4}$$

To complete the formulation, the following boundary conditions are introduced

$$\begin{aligned} &\text{at } y = 0 \quad && u = w = 0, \quad && T = T_w \\ &\text{at } y = \delta \quad && \partial u/\partial y = 0, \quad && \mu(\partial w/\partial y) = \tau_i \end{aligned} \tag{5}$$

$$T = T_s, \qquad \dot{m}_i'' h_{fg} = -k(\partial T/\partial y) \tag{6}$$

where $\dot{m}_i''$ is the interfacial condensation rate per unit area on the condensate film surface. It is given by

$$\dot{m}_i'' = \rho\left(v - u\frac{\partial\delta}{\partial x} - w\frac{\partial\delta}{\partial z}\right)_{y=\delta}. \tag{7}$$

Integration of equation (2) across the film thickness with boundary conditions (5) and (6) yields

$$u = \left[(y/\delta) - \frac{1}{2}(y/\delta)^2\right] g\Delta\rho\delta^2 \sin\phi/\mu. \tag{8}$$

Similarly, integration of equation (3) with respect to y, together with boundary conditions, yields the z-component velocity profile

$$w = \{(\mathrm{d}P/\mathrm{d}z)(y^2/2) + [\tau_i - (\mathrm{d}P/\mathrm{d}z)\delta]y\}/\mu. \tag{9}$$

Also, a linear temperature distribution is obtained from the integration of equation (4) with boundary conditions (5) and (6). This is

$$T = T_w + (T_s - T_w)y/\delta. \tag{10}$$

As discussed in detail in ref. [22] and as shown by Sparrow and Gregg [23], this linear temperature profile is quite valid for small values of Kutateladze number, $Ku \equiv C_p(T_s - T_w)/h_{fg}$ in filmwise condensation. For a few degrees of temperature difference (the usual practice for operations of horizontal evaporators) the value of Ku is less than the order of 10^{-2} for selected fluids such as water, refrigerants and hydrocarbons.

The local film thickness equation can be obtained by integrating the continuity equations with respect to y. Thus

$$\frac{\partial}{\partial x}\int_0^\delta u\,\mathrm{d}y + \frac{\partial}{\partial z}\int_0^\delta w\,\mathrm{d}y = (k/\rho h_{fg})(\partial T/\partial y)_{y=\delta} \tag{11}$$

where the interfacial mass balance equation (6) and the analytic form of condensation rate equation (7) are used. Furthermore, insertion of equations (8), (9) and (10) for u, w and T, respectively, into equation (11) yields a partial differential equation for the local

film thickness distribution, $\delta(\phi, z)$. Thus

$$\left(\frac{2g\rho\Delta\rho}{d}\right)\left(\delta^3\sin\phi\frac{\partial\delta}{\partial\phi}+\frac{\delta^4}{3}\cos\phi\right)-\left(\frac{\rho\delta^2}{\mu}\right)\left(\delta\frac{dP}{dz}-\tau_i\right)\left(\frac{\partial\delta}{\partial z}\right)+\left(\frac{\rho\delta^3}{2\mu}\right)\left(\frac{d\tau_i}{dz}\right)-\left(\frac{\rho\delta^4}{3\mu}\right)\frac{d}{dz}\left(\frac{dP}{dz}\right)-\left(\frac{k\Delta T}{h_{fg}}\right)=0. \quad (12)$$

Solution to this partial differential equation can be obtained to yield $\delta=\delta(\phi,z)$ provided that $\tau_i=\tau_i(z)$, $dP/dz=f(z)$ and the limit of integration $0\le\phi\le\phi_m$ are known. By using the backward finite difference for $(\partial\delta/\partial z)$, $(d\tau_i/dz)$ and (dP/dz), the film thickness partial differential equation reduces to a first-order ordinary differential equation in ϕ. At the tube inlet, $z=0$, the film thickness is assumed to be given by the Nusselt solution. At the top of the tube, $\phi=0$, the film thickness, $\delta(0,z)$, is obtained algebraically from the finite difference form of equation (12). After the film thickness at the top of the tube is obtained, the film thickness along the perimeter for $0<\phi\le\phi_m$ can be solved by the Runga–Kutta method provided that the local pressure gradient, interfacial shear, and stratified angle, ϕ_m, are given. Information about these parameters is discussed in the following sections.

2.3. *Accumulated condensate flow*, $\phi_m<\phi\le\pi$

Assuming the condensate layer to be in laminar motion, the continuity and momentum equations can be simplified as outlined by Chen [22]. They are given as follows:

continuity equation

$$\frac{\partial u}{\partial x}+\frac{\partial v}{\partial y}+\frac{\partial w}{\partial z}=0 \quad (13)$$

axial momentum equation

$$\mu\left(\frac{\partial^2 w}{\partial x^2}+\frac{\partial^2 w}{\partial y^2}\right)-\frac{dP}{dz}=0. \quad (14)$$

Equation (3) can be integrated over the accumulated condensate layer cross-sectional area to yield

$$\frac{d\dot m_l}{dz}=\dot m_l' \quad (15)$$

where $\dot m_l$ is the condensate layer mass flow rate defined as

$$\dot m_l\equiv\iint_{A_l(z)}\rho w\,dA \quad (16)$$

whereas $\dot m_l'$ is the condensate liquid rate per unit axial length that enters the accumulated condensate layer region. $\dot m_l'$ consists of two parts, $\dot m_l'=\dot m_{l1}'+\dot m_{l2}'$. One is due to condensation on the interface of the accumulated layer, $\dot m_{l1}'$, and the other, $\dot m_{l2}'$, is due to the condensing film mass flow that enters the accumulated condensate layer at $\phi=\phi_m$.

A simple energy balance at the interface can be used to calculate $\dot m_{l1}'$ to yield

$$\dot m_{l1}'=h_l(z)d\sin(\pi-\phi_m)(T_s-T_w)/h_{fg} \quad (17)$$

where $h_l(z)$ is the local heat transfer coefficient for the accumulated condensate layer. On the other hand, $\dot m_{l2}'$ can be calculated by integrating the condensate film velocity component, u, given by equation (8) over the film thickness at $\phi=\phi_m$. Thus

$$\dot m_{l2}'=2\int_0^{\delta_m}\rho u\,dy=2g\rho\Delta\rho\delta_m^3\sin\phi_m/3\mu \quad (18)$$

where $\delta_m=\delta_m(z)$ is the condensate film thickness at $\phi=\phi_m$. Incorporating equations (17) and (18) into equation (15), and expressing the resulting equation in terms of superficial volumetric flux, j_{fl}, for the accumulated condensate layer, it can be shown that

$$\frac{dj_{fl}}{dz}=\frac{8g\Delta\rho\delta_m^3}{3\pi d^2\mu}\sin\phi_m+\frac{4h_l\sin(\pi-\phi_m)(T_s-T_w)}{\rho\pi d h_{fg}}. \quad (19)$$

Simplification of equation (14) is achieved by introducing the ratio of the two second derivatives, $r\equiv(\partial^2w/\partial x^2)/(\partial^2w/\partial y^2)$ in equation (14). Thus

$$\partial^2w/\partial y^2=[1/\mu(1+r)](dP/dz). \quad (20)$$

The ratio r in equation (20) can be taken either as a function of the interfacial position, as in Russell *et al.* [17] and Jensen's [24] analyses, or assumed to be a constant as in Buffham's analysis [25]. In a recent analysis of Moalem and Sideman [5], it is assumed that $r\ll1$, and, consequently, the ratio r is completely ignored. In any case as long as r is independent of y, equation (20) can be integrated to solve w provided that no-slip conditions at the tube wall and a relative velocity gradient of τ_i/μ at the gas–liquid interface are used. Furthermore, substituting w in equation (16) yields the condensate layer mass flow rate. Thus

$$j_{fl}=\left(\frac{1}{48\pi\mu}\right)[(-dp/dz)d^2/(1+r)]\times\{2\alpha'^3\beta'-15\alpha'\beta'+(3+12\beta'^2)(\pi-\phi_m)-[4(\tau_i/d)/(dP/dz)](1+r)\times[6\alpha'-2\alpha'^3-6\beta'(\pi-\phi_m)]\} \quad (21)$$

where α' and β' are defined as follows:

$$\alpha'\equiv\sin(\pi-\phi_m);\qquad\beta'\equiv\cos(\pi-\phi_m). \quad (22)$$

In the present analysis, $1/(1+r)=1.05\exp 0.73(\beta'-1)$, is used as suggested by Russell *et al.* [7].

Equation (21) indicates that the liquid flow rate is

related to the angular perimeter of the accumulated condensate layer, ϕ_m, and liquid film thickness δ_m at $\phi = \phi_m$. Consequently, equations (21) and (19) can be solved simultaneously to obtain $\phi_m = \phi_m(z)$ and $j_{fl} = j_{fl}(z)$ provided that other variables such as δ_m, τ_i and (dP/dz) are known. In principle $\delta_m(z)$ can be obtained as a solution for equation (12) whereas calculations of dP/dz and τ_i are obtained from the vapor field balance equations as demonstrated in the following section.

2.4. *Vapor flow field*

The value of the vapor condensation rate can be related to the overall heat transfer. Thus

$$dj_g/dz = 4h(z)(T_s - T_w)/(\rho_g dh_{fg}) \tag{23}$$

where j_g is the superficial volumetric flux for the vapor, and $h(z)$ is the local average heat transfer coefficient.

Neglecting the net momentum exchange between vapor and liquid phases due to phase change, the axial momentum balance for the vapor phase can be used to relate the axial pressure gradient to interfacial shear. Thus

$$\frac{dP}{dz} = -(4\tau_i/d_h) - \rho_g j_g \frac{d}{dz}(j_g/\alpha) \tag{24}$$

where d_h is the hydraulic diameter for the vapor phase and α is the void fraction. They are defined as $d_h = 4A_g/\xi_i$ and $\alpha \equiv A_g/A$. The vapor cross-section, A_g, and the corresponding vapor-phase circumferential perimeter, ξ_i, are related to the peripheral angle, ϕ_m, of the condensate layer angle by

$$A_g = d^2(2\phi_m - \sin 2\phi_m)/8,$$
$$\xi_i = d[\phi_m + \sin(\pi - \phi_m)]. \tag{25}$$

The interfacial shear is calculated locally based on the local vapor velocity as $\tau_i = f_i(\rho_g w_g^2/2)$ with the vapor-phase interfacial friction factor, f_i, and the average vapor velocity, w_g, respectively given by $f_i = c\,Re_g^{-m}$ and $w_g = j_g/\alpha$. Where c and m are given as $c = 0.046$ and $m = 0.2$ for turbulent vapor flow, $c = 16$ and $m = 1.0$ for laminar vapor flow. The vapor flow regime is determined by the local value of vapor Reynolds number, $Re_g \equiv w_g d_h/\nu_g$.

In view of equations (23) and (24), j_g, τ_i and (dP/dz) can be calculated, respectively. Equation (12) can now be solved for $\delta(\phi, z)$ provided that the local averaged heat transfer coefficient, $h(z)$, is known.

2.5. *Local and averaged heat transfer coefficient*

As illustrated in the preceding section the hydrodynamic fields in the peripheral thin liquid film and the relatively thick condensate layer at the bottom of the tube are quite different from each other. Therefore, the heat transfer process in these two regions should be modeled differently.

In view of equation (10), the local heat flux at the condensate film is given as

$$q_c''(\phi, z) = k[T_s(z) - T_w]/\delta(\phi, z). \tag{26}$$

The local heat transfer coefficient for the condensate film can be calculated as

$$h_c(\phi, z) = k/\delta(\phi, z) \quad \text{for } 0 \le \phi \le \phi_m. \tag{27}$$

Now, equation (27) can be used to evaluate the local average heat transfer coefficient, $h_c(z)$, as follows:

$$h_c(z) = \frac{1}{\phi_m}\int_0^{\phi_m} h_c(\phi, z)\,d\phi$$
$$= \frac{k}{\phi_m}\int_0^{\phi_m} [1/\delta(\phi, z)]\,d\phi. \tag{28}$$

Equations (27) and (28) can be used to evaluate $h_c(\phi, z)$ and $h_c(z)$ by using $\delta(\phi, z)$ obtained from equation (12). Since it is expected that $\delta(\phi, z)$ increases as ϕ increases, the local heat transfer coefficient for the condensate film decreases inversely with the angular position.

The heat transfer coefficient for the accumulated condensate layer has been extensively studied in the literature [3, 7, 8, 26]. It was found that the heat transfer coefficient for the accumulated condensate layer is negligibly small as compared to the heat transfer coefficient, h_c, at the upper portion of the tube. In almost all analyses associated with condensation in horizontal or near horizontal pipes, the contribution of the condensate layer to the overall heat transfer coefficient at any axial distance, z, is completely neglected. For the purpose of completeness, Rossen and Myers' [13] analytical prediction for the heat transfer coefficient, $h_l(z)$, for the condensate layer is utilized here. It is based on von Karman's analogy, and is given by

$$h_l(z) = \frac{\Phi_l(k/d)(8Re_{sl})^{1/2}}{5 + 5[\ln(5Pr + 1)]Pr^{-1}} \tag{29}$$

where Φ_l is the square root of the two-phase frictional pressure drop multiplier. The predictions obtained from equation (29) were compared by Rossen and Myers with their experimental measurements, and the comparison was found to yield a very good agreement. This is the reason why equation (29) is preferred in this study.

Using the present condensate film heat transfer solution of equation (28) and Rossen and Myers' prediction for the accumulated condensate layer, the overall local average heat transfer coefficient, $h(z)$, at any axial location in the tube is obtained by

$$h(z) = [\phi_m h_c(z) + (\pi - \phi_m)h_l(z)]/\pi. \tag{30}$$

This heat transfer coefficient is based on the local temperature difference $\Delta T(z) \equiv T_s(z) - T_w$. It is convenient to define the heat transfer coefficient based on the inlet temperature difference $\Delta T_i \equiv T_{si} - T_w$

rather than the local one. The local average heat transfer coefficient based on the inlet temperature can be expressed as

$$h_i(z) = [\Delta T(z)/\Delta T_i]h(z). \quad (31)$$

The overall average heat transfer coefficient is obtained by integrating equation (31) over the entire tube length, l. Hence, the overall average heat transfer coefficient, h, is given by

$$\bar{h} = (1/l)\int_0^l h_i(z)\,dz. \quad (32)$$

3. GENERAL OUTLINE OF SOLUTION PROCEDURE

Given the standard design data, the calculation of local and average heat transfer coefficients proceeds in a stepwise manner as follows.

(1) Starting at the tube inlet, $z = 0$, with pure vapor entering the tube, the inlet condensate film thickness and heat transfer coefficient can reasonably be approximated by Nusselt's solution. Nusselt's solution gives the accumulated condensate layer rate, j_{fl}, and the reduced vapor volume flow rate, j_g, in the first increment of Δz.

(2) The present heat transfer analysis starts at $z = \Delta z$. The vapor shear and pressure gradient based on the inlet condition or the previous axial position for the subsequent increments are initially utilized to solve the stratified angle, ϕ_m, from equation (21). After obtaining a tentative value of ϕ_m, the local values of α, w_g, d_h, τ_i, dp/dz, $p(z)$, $T_s(z)$ and Φ_l can be calculated in order. The new values of τ_i, dp/dz and the fluid properties are used to resolve the stratified angle. The iteration process is terminated when the results of two successive values of ϕ_m agree to within a specified tolerance.

(3) Using the backward finite differences form of equation (12), the computation of the local condensate film thickness, $\delta(\phi, z)$, at the same axial position, z, proceeds from $\phi = 0$ along the periphery until ϕ reaches the pre-obtained value of ϕ_m from step 2. Then, the local heat transfer coefficients $h_c(\phi, z)$, $h_c(z)$, $h_l(z)$, $h(z)$ and $h_i(z)$ can be calculated from equations (27)–(31), respectively.

(4) The accumulated condensate layer flux, j_{fl}, and the vapor flux, j_g, at the end of this step are obtained by

$$j_{fl}(z + \Delta z) = j_{fl}(z) + \frac{dj_{fl}}{dz}\Delta z \quad (33)$$

and

$$j_g(z + \Delta z) = j_g(z) - \frac{dj_g}{dz}\Delta z \quad (34)$$

where (dj_{fl}/dz) and (dj_g/dz) are given by equations (19) and (23), respectively.

(5) Steps 2–4 are repeated to solve for the film thickness and heat transfer coefficients at $z = z + \Delta z$, and then the solution proceeds with the next axial position.

(6) The numerical calculation procedure is halted when $T_s(z) \leq T_w$ or if $j_g(z) = 0$.

(7) Finally, the overall average heat transfer coefficient, h, is obtained by integration of the local values of $h_i(z)$ as indicated in equation (32).

4. RESULTS AND DISCUSSION

The present study represents an attempt to predict the local and average values of the heat transfer coefficients in the axial, as well as in the peripheral, direction, while accounting for the interfacial shear, axial pressure variations, saturation temperature level, inlet subcooling and vapor flow rates. Since the solution is obtained numerically, it is interesting to note the characteristics and point values of the basic variables affecting the condensation heat transfer coefficient, and to compare the results with available experimental data when it is possible.

The axial pressure gradient obtained from equation (24) is presented in Figs. 2 and 3. Figure 2 represents the local pressure gradient at four inlet saturation temperature levels while keeping the vapor inlet Reynolds number, Re_{gi}, and inlet subcooling, ΔT_i, constant. Although pressure recovery resulting from vapor deceleration (the second term on the right-hand side of equation (24)) is higher as the temperature level decreased, due to the much larger adverse effect of the frictional pressure gradient the overall pressure gradient decreases with decreasing temperature. The same conclusion was noted by Moalem and Sideman [5]. However, they obtained a higher decrease in the pressure gradient because of the pressure recovery effect which was not taken into account in their analysis. Furthermore, it is to be noted that due to the relatively higher vapor flow rates at the entry region of the vapor the temperature level effect is more pronounced at this region. The parametric effects of inlet temperature difference, ΔT_i, and vapor flow rate on the axial pressure gradient are demonstrated in Fig. 3. As indicated by the curves in this figure, higher ΔT_i and lower vapor flow rates yield higher pressure gradients.

Since the local saturation temperature inside the tube is affected by the local pressure gradient, it is interesting to see the variation of the local temperature difference, $\Delta T(z) \equiv T_s(z) - T_w$, along the tube associated with the temperature levels used to construct Fig. 2. As shown in Fig. 4, the dimensionless local subcooling, $(\Delta T/\Delta T_i)$, decreases along the tube length since the local saturation temperature is gradually reduced. As expected from Fig. 2, $\Delta T/\Delta T_i$ is significantly reduced with the decreasing temperature level since a lower saturation temperature produces a greater pressure drop. Although it is not shown here,

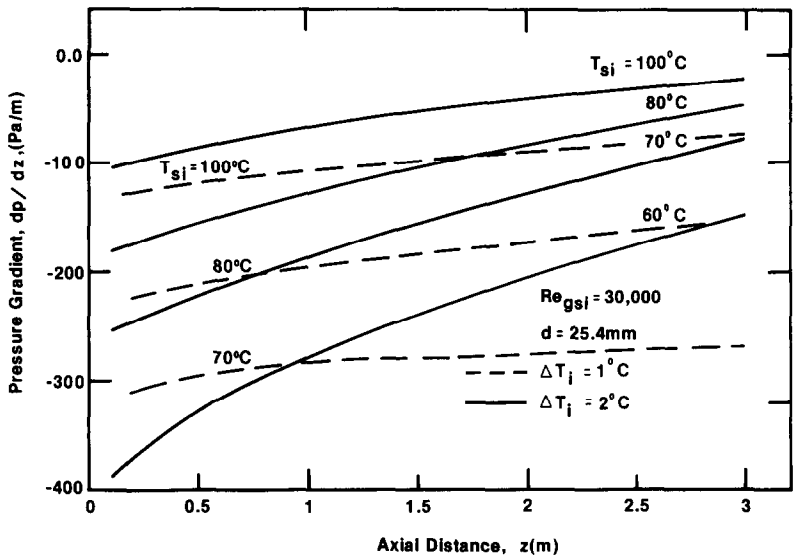

FIG. 2. Variation of pressure gradient in axial direction at various inlet condensation temperatures for water–steam flow.

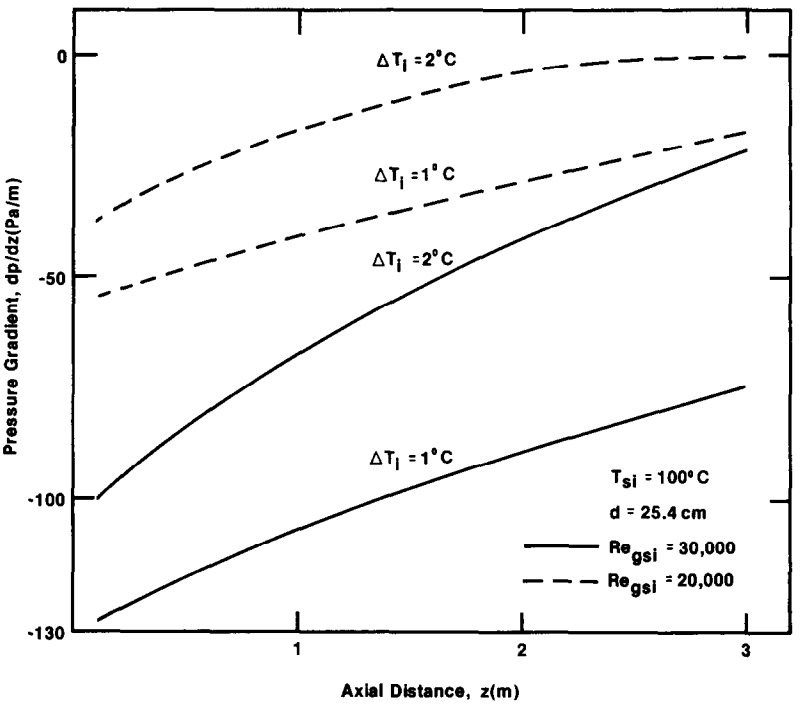

FIG. 3. Variation of pressure gradient along the tube at various inlet Reynolds numbers and inlet temperature differences for water–steam flow.

increasing the inlet subcooling yields an increase in the dimensionless local subcooling along the tube axis. However, the increase is not significant enough to produce the results obtained here.

Figure 5 represents the liquid film thickness along the periphery of the tube at various axial distances. When compared with the Nusselt type solution where the effect of interfacial shear is neglected, the present solution yields a thicker condensate film along the periphery. It is interesting to note that although the effect of interfacial shear is small in general terms it is more pronounced at the entry region where the

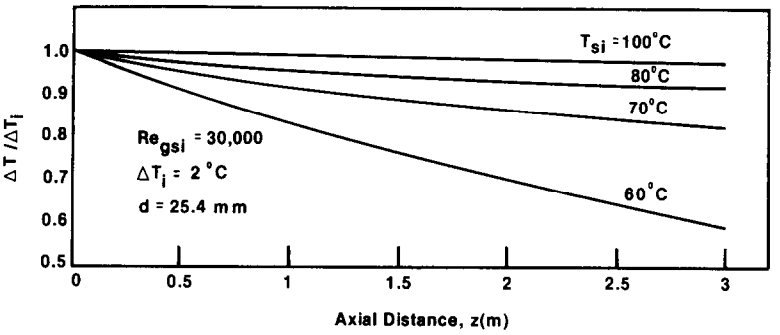

FIG. 4. Variation of temperature difference along the tube at various inlet condensation temperatures for water–steam flow.

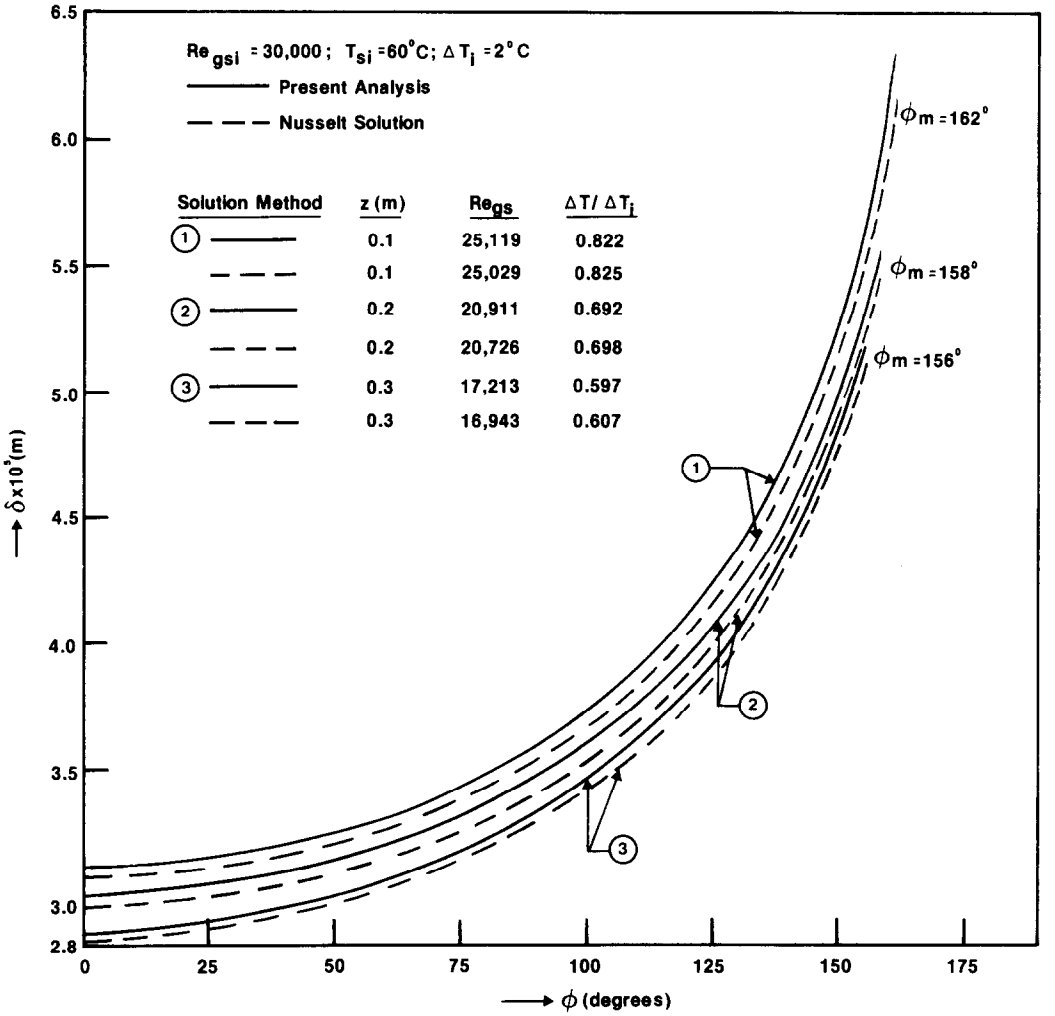

FIG. 5. Development of condensate film thickness along the tube periphery at various axial positions for water–steam flow.

vapor flow rate is the highest. Furthermore, it is noted that the higher pressure drop obtained from the present analysis causes higher temperature drops than those obtained from the Nusselt solution.

Figure 6 represents the effects of the pipe inlet temperature difference, ΔT_i, and the vapor flow rate on the stratified angle, ϕ_m, or on the height of the accumulated condensate layer, H/d, at the bottom of the tube. As indicated by the curves in this figure, an increase in the inlet subcooling (while keeping the vapor flow Reynolds number based on the pipe inlet conditions, Re_{gi}, constant) yields, due to a higher condensation rate, a smaller stratified angle or a thicker accumulated condensate layer. The effect of

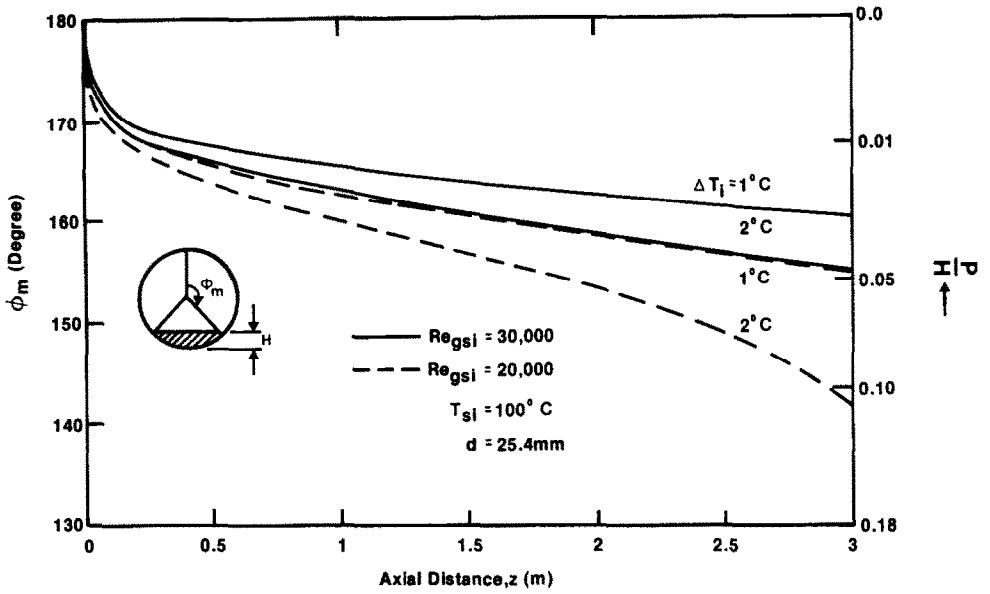

FIG. 6. Variation of stratified angle along the tube at various temperature differences and vapor flow rates for water–steam flow.

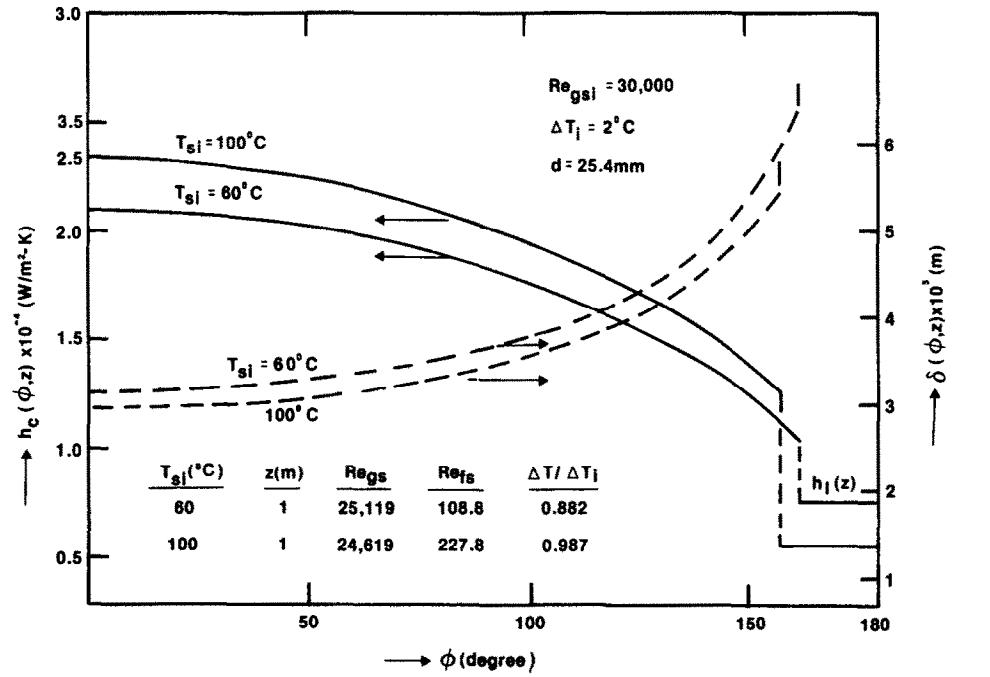

FIG. 7. Variation of local condensate film heat transfer coefficient along the periphery at various inlet subcoolings for water–steam flow.

the inlet subcooling level is increased as the vapor flow rate is decreased and the axial distance is increased. On the other hand the stratified angle is increased with vapor flow rate. This may be due to the greater interfacial shear resulting in a thinner accumulated condensate layer.

The variations of the local condensate film heat transfer coefficient, $h_c(\phi, z)$, along the periphery of the tube at $z = 1$ m are presented in Figs. 7 and 8. The first figure demonstrates the effect of the inlet subcooling on $h_c(\phi, z)$ whereas the second one shows the effect of the inlet saturation temperature level. Two interesting results are observed. The first is that for a given value of ΔT_i or T_{si}, the local heat transfer coefficient is continuously decreasing along the periphery until the stratified angle is attained, and drops to the accumulated condensate layer heat transfer coefficient level, $h_l(z)$, as given by equation (29). The

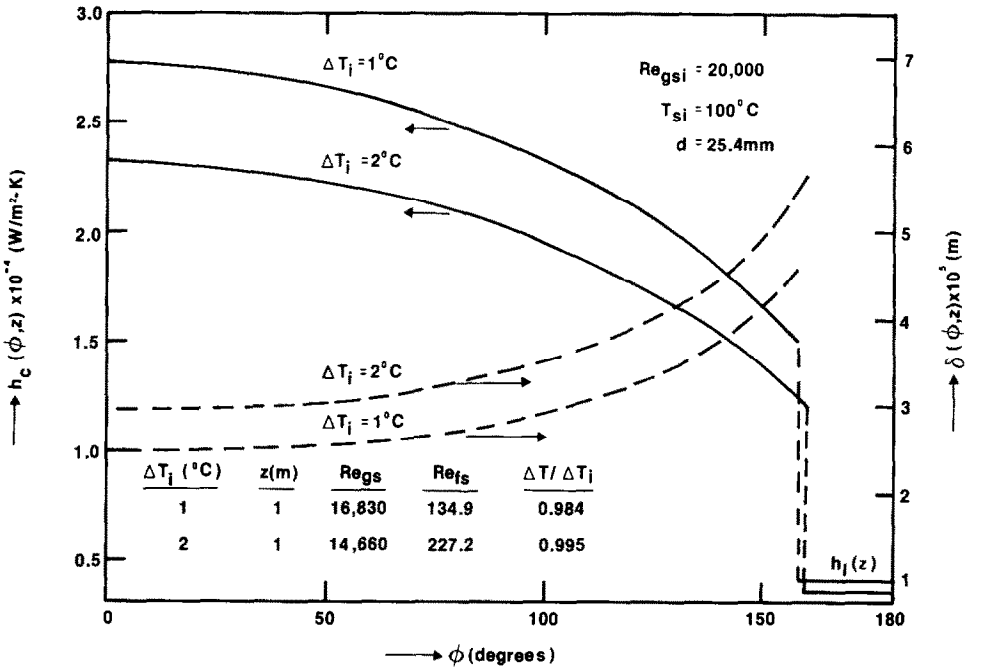

FIG. 8. Variation of local condensate film heat transfer coefficient along the periphery at various saturation temperatures for water–steam flow.

second is that higher saturation temperature levels and lower inlet subcooling yield higher heat transfer coefficients. Both phenomena are understandable in view of the associated peripheral film thickness characteristics and the condensate layer thickness. Lower ϕ_m (or higher condensate layer thickness) associated with higher T_{si} leads to apparently higher heat transfer coefficients since the transfer area for the condensate film is smaller. It must, however, be emphasized here that the sudden drop from $h_c(\phi_m, z)$ to $h_l(z)$ is not expected in reality. This is due to the analytical model presented here which assumes two region calculations, one for $0 \leq \phi \leq \phi_m$ and the other for $\phi_m < \phi \leq \pi$. The analytical model allows local peripheral calculations for the first region and an average calculation for the second one.

Figure 9 represents and compares the peripherally averaged condensate film heat transfer coefficient, $h_c(z)$, as predicted by equation (28), the average condensate layer heat transfer coefficient, $h_l(z)$, as predicted by equation (29) and, finally, the local average heat transfer coefficient, $h(z)$, as predicted by equation (31). As is indicated by the curves in this figure, an increase in the temperature level and axial distance yields a higher condensate film heat transfer coefficient. This phenomenon is understandable in view of the associated film thickness characteristics and local temperature differences as demonstrated by Figs. 8 and 4, respectively. Also, in view of the higher pressure gradients, i.e. higher value of Φ_1, associated with lower temperature levels as indicated by Fig. 2, the corresponding condensate layer heat transfer coefficients obtained by equation (29) are higher at lower temperatures. However, due to the interacting effects of T_{si}, ΔT_i, dp/dz and ϕ_m it is impossible to comment on the overall behavior of $h(z)$ which is based on the local temperature difference, ΔT_i. With regard to low temperature behavior the only explanation can be given in terms of the significant drop in ΔT_i as evidenced by Fig. 4. In contrast to the behavior of $h(z)$, Fig. 10 shows a consistent trend for $h_i(z)$, the local heat transfer coefficient based on the inlet temperature difference, ΔT_i. Higher temperature levels yield higher $h_i(z)$ with the more pronounced effects at relatively low temperatures. Furthermore, a consistent decrease in the axial direction may be attributed to the pressure drop, the decreasing vapor flow rate, and the decreased stratified angle in the axial direction.

Due to lack of experimental data on the local values of various parameters associated with the condensation heat transfer in horizontal pipes, the validity of the theoretical results presented above cannot be checked with experimental data. However, the overall average heat transfer coefficient, h, predicted by equation (32) is compared with the available experimental data in Fig. 11. The experimental data source used for this comparison is listed in Table 1. The table includes the data of Deans [27], Crosser [28], Rossen [29], Myers [26], Luu [30] and Jaster and Kosky [10]. Test fluids used in these experiments include Freon-12, Freon-113, water, methanol, acetone and propane. These data cover a wide range of physical properties, flow parameters and tube sizes. The data used in this comparison are limited by the stratified-smooth and stratified-wavy two-phase flow patterns where the present theory holds. In order to be sure that the data points are comparable with

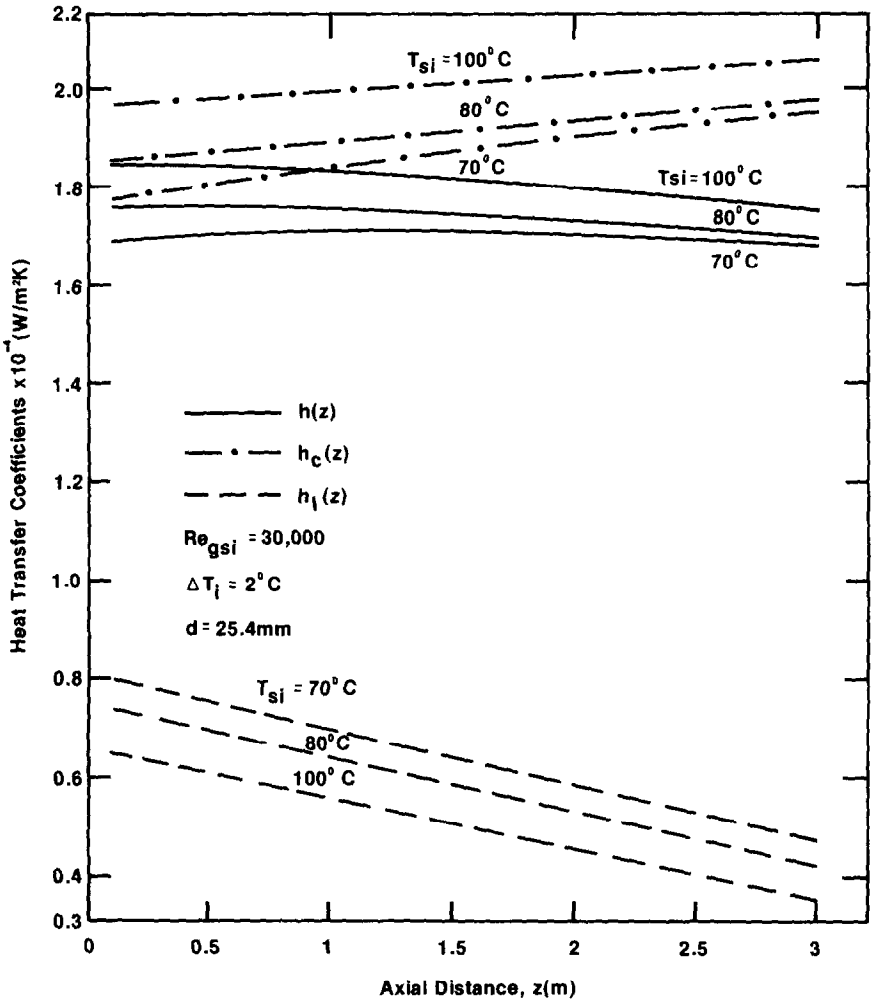

FIG. 9. Axial variation of local averaged heat transfer coefficients at various saturation temperatures for water–steam flow.

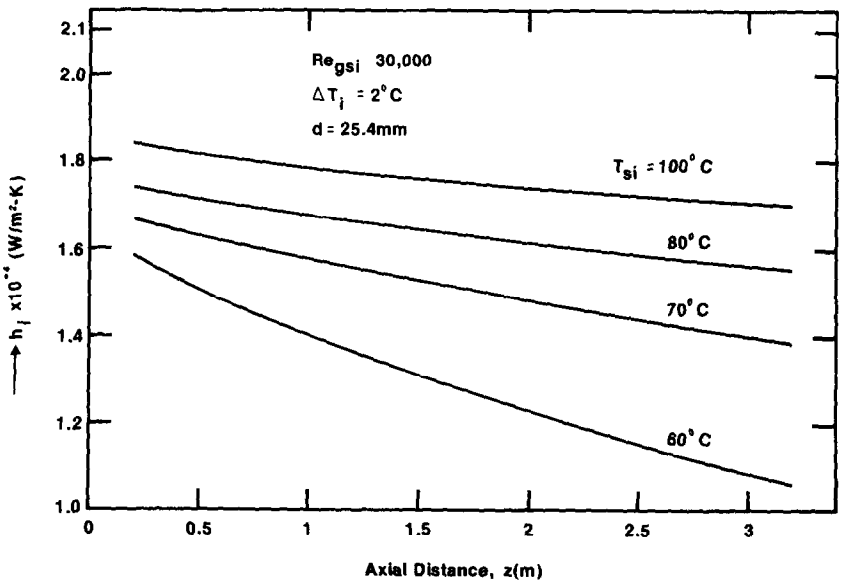

FIG. 10. Variation of local averaged heat transfer coefficient based on the inlet temperature difference along the tube axis at various saturation temperatures for water–steam flow.

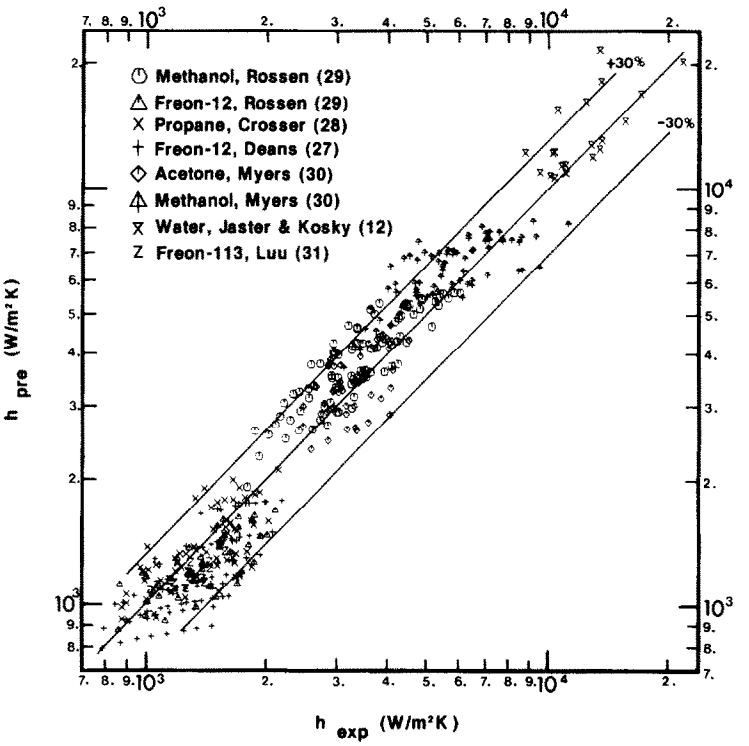

FIG. 11. Comparison of overall heat transfer coefficient predicted by the present analysis with available experimental data.

Table 1. Condensation data sources

References	Fluid	d (cm)	l (m)	No. of data points	Pre-condensate flow
Deans [27]	F-12	1.58	1.433	84	No
Crosser [28]	Propane	1.58	1.433	65	No
Rossen [29]	Methanol	1.66	0.3	86	Yes
Rossen [29]	F-12	1.66	0.3	38	Yes
Myers [26]	Methanol	1.08	0.38	78	Yes
Myers [26]	Acetone	1.08	0.38	48	Yes
Jaster and Kosky [10]	Steam	1.25	0.42	21	Yes
Luu [30]	F-113	1.34	3.65	17	No

theoretical predictions, each data point is checked by the Taitel and Dukler flow-pattern transition criteria [18]. The comparison furthermore is restricted to reported publications where all the experimental variables required for the theoretical calculations were presented. For example, the condensation data of Kutateladze [14], Chato [8] and Kroger [16] are not included in this comparison because pertinent flow conditions are not specified in these references. In view of these restrictions, Fig. 11 shows that the experimental data points scatter around the present predictions with a maximum discrepancy of 30% with a mean deviation of 15.5%. It is worthwhile to point out here that a few points of Crosser's lower heat transfer data were observed with a zero vapor flow rate at the tube exit indicating vapor condensation had ceased before the end of the tube and may cause these extremely low heat transfer measurements.

Taking into account the reported experimental errors for the experimental data which are about 7–20%, the predictions presented in Fig. 11 have a good agreement with the overall experimental data for a wide range of experimental conditions.

5. HEAT TRANSFER CORRELATION

In the preceding sections heat transfer analysis has been carried out for the purpose of predicting heat transfer coefficients for condensation inside horizontal tubes. Numerical solutions have been performed to demonstrate the parametric effects of various fluid and flow variables. However, the numerical methods which are required by the present analysis may not be convenient for practical purposes. Here, an attempt is made to obtain a simple correlation for predicting

the overall average heat transfer coefficient for condensation inside horizontal tubes.

In attempting to develop a general correlation, one can either determine the correlation from a set of experimental data, or build up a physical model and derive a correlation from its numerical solution; and then compare it to the experimental data, and if necessary, correct this theoretically based correlation by empirical factors. So far only a few sets of well-defined condensation data are available, and most of these do not include all possible variables which may affect the heat transfer coefficient. Moreover, some of the essential variables utilized in these tests do not cover a wide enough range; and, hence, the available data are not sufficient for building up a valid correlation. Additional experiments would be required to form useful correlations. In view of these difficulties, it is not convenient to obtain a working correlation based on experimental data. Therefore, the second method based on modeling will be followed here to obtain a practical correlation from the numerical solution of the present model described in the preceding sections.

The overall heat transfer coefficient is influenced by the transfer processes occurring in the peripheral condensate film and the accumulated condensate layer at the bottom of the tube. However, as demonstrated by Fig. 9, the condensate layer heat transfer coefficient is much smaller than the condensate film heat transfer coefficient. The contribution of the condensate layer to the overall heat transfer is further reduced by equation (30) because it is weighed by a factor of $(\pi - \phi_m)/\phi_m$ which is much less than unity. These two arguments indicate that the overall heat transfer coefficient is governed by the condensate film heat transfer, which is directly proportional to (k/δ) by equation (27). Therefore, the differential equation for the film thickness, equation (12), can be used to obtain the characteristic dimensionless groups affecting the heat transfer.

Introducing the dimensionless quantities, $\delta^+ \equiv \delta/d$, $z^+ \equiv z/d$, $\tau_i^+ \equiv \tau_i/\tau_{ir}$, $\Delta p^+ \equiv \Delta p/(\tau_{ir} l/d)$ and $\Delta T^+ \equiv \Delta T/\Delta T_r$ into equation (12), it can be shown that in dimensionless form equation (12) is given by

$$2\left(\delta^{+3}\sin\phi\frac{\partial\delta^+}{\delta\phi}+\frac{\delta^{+4}}{3}\cos\phi\right)-\left(\frac{\tau_{ir}}{g\Delta\rho d}\right)\left[\delta^+\left(\frac{l}{d}\right)\frac{dp^+}{dz^+}-\tau_i^+\right]\left(\frac{\partial\delta^+}{\partial z^+}\right)+\left(\frac{1}{2}\right)\left(\frac{\tau_{ir}}{g\Delta\rho d}\right)\delta^{+3}\frac{d\tau_i^+}{dz^+}-\frac{1}{3}\left(\frac{\tau_{ir}}{g\Delta\rho d}\right)\frac{d^2p^+}{dz^{+2}}-\frac{Ku}{Pr\,Ga^3}\Delta T^+=0 \quad (35)$$

where τ_{ir} and ΔT_r are reference scales for τ_i and ΔT, respectively. For the purpose of convenience, tube inlet values of τ_i and ΔT can be taken as reference shear and temperature difference. It is important to note from equation (35) that the characteristic dimensionless groups which affect the heat transfer process are the Kutateladze number, $Ku \equiv C_p\Delta T_r/h_{fg}$, liquid Prandtl number, $Pr \equiv \rho C_p \nu/k$, Galileo number, $Ga \equiv d(g\Delta\rho/\rho\nu^2)^{1/3}$, dimensionless interfacial shear, $\tau_{ir}/g\Delta\rho d$, and (l/d) ratio. In view of equation (35), it can be inferred that the Nusselt number based on the overall heat transfer coefficient can be expressed as

$$\overline{Nu} \equiv \bar{h}k/d = f(Ku, Pr, Ga, l/d, \tau_{ir}/\rho g d). \quad (36)$$

However, considering the fact that the interfacial shear can be expressed in terms of the vapor Reynolds number and that there may exist some liquid at the entrance, equation (36) can be cast into the following form

$$\overline{Nu} = f(Ku, Pr, Ga, l/d, Re_{gsi}, Re_{lsi}) \quad (37)$$

where $Re_{gsi} \equiv j_{gi}d/\nu_g$ and $Re_{lsi} \equiv j_{li}d/\nu$ are the inlet superficial Reynolds numbers for vapor and liquid flow, respectively.

By using a multiple linear regression method, numerical solution described in the preceding sections is correlated in the following simple form:

$$\overline{Nu} = 0.492\,Ku^{-0.27}\,Pr^{0.25} \times Ga^{0.73}(l/d)^{-0.03} \times Re_{gsi}^{0.05}(1 + Re_{lsi})^{-0.01}. \quad (38)$$

Figure 12 compares the heat transfer coefficients calculated from the correlation, equation (38), with the present numerical predictions for the condensation data listed in Table 1. The comparison between the present numerical solution and the predictions by the proposed correlation is shown to have a very good agreement with a mean deviation of about 2.8%. This confirms that the numerical solution developed in this study can be well represented by the proposed correlation.

Figure 13 compares the predictions by the proposed correlation with the available experimental data of more than 400 points. From this figure it can be observed that most of the predicted results agree with the experimental data with a maximum of discrepancy of $\pm 30\%$ and with an overall mean deviation of about 16.2%. It should be noted here that the experimental data used for this comparison have reported measured errors of about 7–20%. Furthermore, it is important to note here that the experimental data used in this comparison cover a wide range of values of the characteristic dimensionless groups. These can be summarized as follows:

$0.002 \le Ku \le 0.1$; $\quad 18 \le l/d \le 269$

$1.5 \le Pr \le 6.1$; $\quad 3000 \le Re_{gsi} \le 300{,}000$

$400 \le Ga \le 1500$; $\quad 0 \le Re_{fsi} \le 2000$.

In view of the favorably good agreement between the correlative predictions and experimental data and

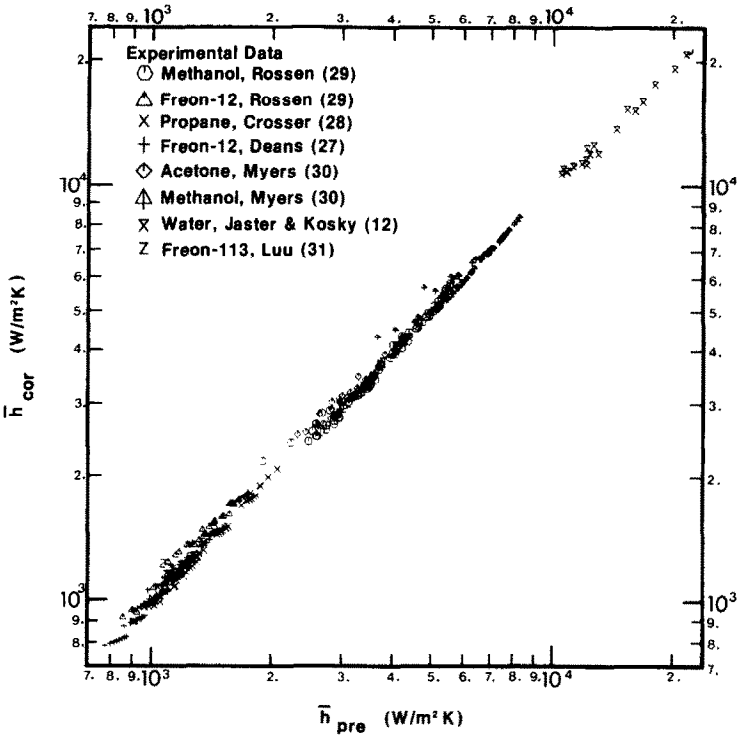

FIG. 12. Comparison of overall heat transfer coefficient predicted by the present analysis with the proposed correlation.

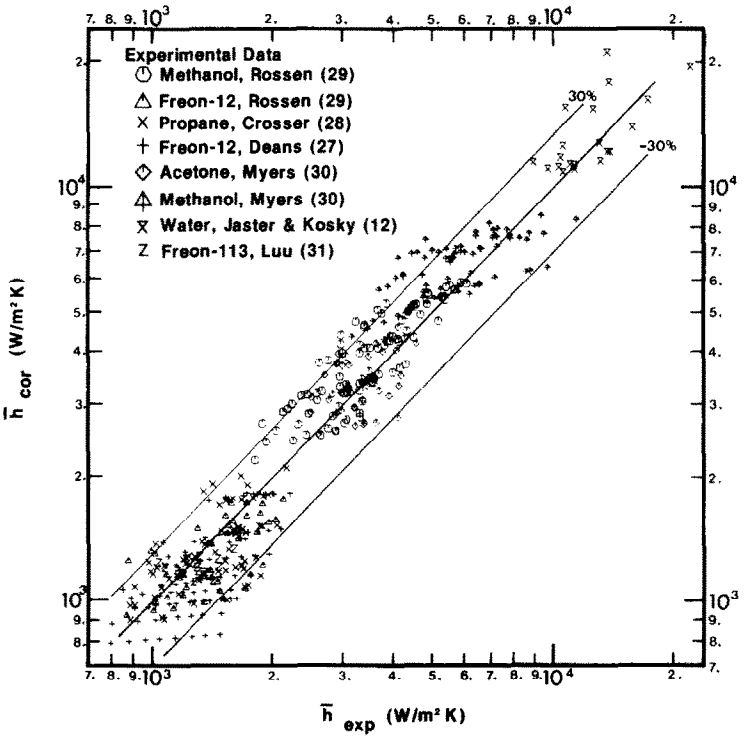

FIG. 13. Comparison of overall heat transfer coefficient predicted by the proposed correlation with available experimental data.

in view of the wide range of experimental data used in this comparison, the proposed correlation can be safely used in predicting the overall heat transfer coefficient for the practically interesting laminar flow range of operating conditions of the condensation process inside horizontal tubes.

6. SUMMARY AND CONCLUSIONS

An analysis has been carried out for the purpose of predicting heat transfer coefficients for condensation inside horizontal tubes. The analysis took into account the effects of interfacial shear, axial pressure gradient, saturation temperature levels, driving temperature difference and the development of the stratified angle associated with the accumulated condensate layer at the bottom of the tube. Numerical solutions have been performed to demonstrate the parametric effects of various fluid and flow variables for the laminar, and practically interesting, range of operating conditions of water-vapor flow. A theoretical predictive method is developed to obtain the overall heat transfer coefficient along the tube length.

Results of the theoretical predictions were shown to have a good agreement with the reported experimental data which cover a variety of fluids with a relatively wide range of operating conditions.

Finally, a simple, predictive heat transfer correlation was developed from the numerical solutions by means of regression analysis. It was shown that the predictions obtained from the proposed correlation was as good as those obtained from the theoretical solution. This fact indicates that the dimensionless groups included in the correlation are representative of the heat transfer process associated with condensation inside horizontal tubes. This correlation can be applied with confidence for the stratified, cocurrent flow of laminar condensate liquid.

REFERENCES

1. K. J. Bell, J. Taborek and F. Fenoqlio, Interpretation of horizontal in-tube condensation heat transfer correlation with a two-phase flow regime map, *Chem. Engng Prog. Symp. Ser.* **66**, 150–156 (1970).
2. I. H. Newson, Heat transfer characteristics of horizontal tube multiple effect evaporators—possible enhanced tube profiles, *Proceedings 6th International Symposium Fresh Water from the Sea*, Vol. 2, pp. 113–124 (1978).
3. D. Moalem and S. Sideman, Theoretical analysis of a horizontal condenser–evaporator tube, *Int. J. Heat Mass Transfer* **19**, 259–270 (1976).
4. D. Moalem and S. Sideman, Theoretical analysis of a horizontal condenser–evaporator elliptical tube, *Trans. ASME*, Series C, *J. Heat Transfer* **92**, 352–359 (1975).
5. D. Moalem and S. Sideman, Condensation inside near horizontal tubes in co-current and counter-current flow, *Int. J. Heat Mass Transfer* **25**, 1439–1444 (1982).
6. W. Nusselt, Die Oberflachenkandensation des Wasser Dampfes, *Z. Ver. dt. Ing.* **60**, 541–575 (1916).
7. J. B. Chaddock, Film condensation of vapors in horizontal tubes, *Refrigng Engng* **65**, 36–41 and 90–95 (1957).
8. J. C. Chato, Laminar condensation inside horizontal and inclined tubes, *ASHRAE Jl* **4**, 52–60 (1962).
9. C. E. Rufer and S. O. Kezios, Analysis of two-phase one component stratified flow with condensation, *J. Heat Transfer* **88c**, 265–275 (1965).
10. H. Jaster and P. G. Kosky, Condensation heat transfer in a mixed flow regime, *Int. J. Heat Mass Transfer* **19**, 95–99 (1976).
11. W. W. Akers, H. A. Deans and O. K. Crosser, Condensing heat transfer in horizontal tubes, *Chem. Engng Prog. Symp. Ser.* **55**, 171–176 (1959).
12. W. W. Akers and H. F. Rossen, Condensation inside a horizontal tube, *Chem. Engng Prog. Symp. Ser.* **56**, 145–149 (1960).
13. H. F. Rossen and J. A. Myers, Point values of condensing film coefficients inside a horizontal pipe, *Chem. Engng Prog. Symp. Ser.* **61**, 190–199 (1965).
14. S. S. Kutateladze, Heat transfer during film condensation of vapor inside a horizontal tube. In *Problems of Heat Transfer and Hydraulics of Two-phase Media*, pp. 162–180. Pergamon Press, Oxford (1961).
15. A. S. P. Sarma, P. K. Sarma and I. Venkata Apparav, An empirical correlation for condensation heat transfer under one component stratified flow conditions, *Can. J. chem. Engng* **50**, 541–543 (1972).
16. D. G. Kroger, Laminar condensation heat transfer inside inclined tubes, *Chem. Engng Prog. Symp. Ser.* **73**, 256–260 (1976).
17. T. W. F. Russell, A. W. Etchells, R. H. Jensen and P. J. Arruda, Pressure drop and hold-up in stratified gas–liquid flow, *A.I.Ch.E. Jl* **20**, 664–669 (1974).
18. Y. Taitel and A. E. Dukler, A model for predicting flow regime transitions in horizontal and near horizontal gas–liquid flow, *A.I.Ch.E. Jl* **22**, 44–75 (1976).
19. G. Breber, J. W. Palen and J. Taborek, Prediction of horizontal tube-side condensation of pure components using flow regime criteria, *J. Heat Transfer* **102**, 471–476 (1980).
20. R. G. Sardesai, R. G. Owen and D. J. Pulling, Flow regimes for condensation of a vapor inside a horizontal tube, *Chem. Engng Sci.* **36**, 1173–1180 (1981).
21. D. Butterworth, An analysis of film flow and its application to condensation in a horizontal tube, *Int. J. Multiphase Flow* **1**, 671–682 (1974).
22. I. Y. Chen, Heat transfer analysis of a falling-film horizontal tube evaporator, Doctoral Thesis, University of Wisconsin—Milwaukee, Milwaukee, Wisconsin (1984).
23. E. M. Sparrow and J. L. Gregg, A boundary layer treatment of laminar film condensation, *J. Heat Transfer* **81**, 13–18 (1959).
24. R. H. Jensen, Stratified two-phase flow in horizontal pipelines, M.S. Thesis, University of Delaware, Newark (1972).
25. B. A. Buffham, Laminar flow in open circular channels and symmetrical lenticular tubes, *Trans. Instn chem. Engrs* **46**, 152–157 (1968).
26. J. A. Myers, Condensation inside a horizontal pipe, studied with a heat meter, Ph.D. Thesis, University of Kansas, Lawrence, Kansas (1964).
27. D. A. Deans, Heat transfer coefficient for Freon-12 condensing within a horizontal tube, Master's Thesis, Rice Inst., Houston, Texas (1955).
28. D. K. Crosser, Condensing heat transfer within horizontal tube, Ph.D. Thesis, Rice Inst., Houston, Texas (1955).
29. H. F. Rossen, Heat transfer during condensation inside a horizontal tube, Ph.D. Thesis, Rice Inst., Houston, Texas (1957).
30. M. Luu, Augmentation of in-tube condensation, Ph.D. Thesis, Iowa State University (1980).

TRANSFERT THERMIQUE PAR CONDENSATION POUR L'ECOULEMENT DIPHASIQUE STRATIFIE A COCOURANT DANS LES TUBES HORIZONTAUX

Résumé—On étudie le transfert thermique par condensation dans les tubes horizontaux pour l'écoulement cocourant stratifié de vapeur et de liquide. L'analyse tient compte des effets du cisaillement à l'interface, du gradient de pression axial, du niveau de la température de saturation, de la différence de température et de l'angle associé à la couche de condensat accumulée à la base du tube. L'influence de ces paramètres est évaluée par référence au transfert thermique du film périphérique de condensat pour les domaines pratiques d'écoulement laminaire d'eau et vapeur d'eau. Une méthode théorique prédictive est développée pour obtenir le coefficient global de transfert le long du tube. Les calculs s'accordent avec les données expérimentales qui couvrent une variété de fluides pour des conditions opératoires relativement étendues. Une formule simple est proposée pour prévoir le transfert thermique; elle est déduite d'une analyse de régression portant sur les résultats du calcul.

WÄRMEÜBERGANG BEI DER KONDENSATION IN EINER GESCHICHTETEN, GLEICHGERICHTETEN ZWEIPHASENSTRÖMUNG IN EINEM WAAGERECHTEN ROHR

Zusammenfassung—Der Wärmeübergang bei der Kondensation in waagerechten Rohren wird für geschichtete, gleichgerichtete Strömung von Dampf und Flüssigkeit untersucht. Dabei werden insbesondere die Einflüsse der Oberflächenschubspannung, des axialen Druckgradienten, der Sättigungstemperatur, der treibenden Temperaturdifferenz und die Ausbildung des Schichtungswinkels des Kondensates am Rohrgrund betrachtet. Die Parameter wirken sich im praktisch interessierenden laminaren Bereich auf die Verteilung des Wärmeüberganges am Rohrumfang aus. Ein theoretisches Berechnungsverfahren zur Bestimmung des Gesamtwärmeübergangskoeffizienten in Rohrlängsrichtung wird entwickelt. Die experimentellen und theoretischen Ergebnisse stimmen für eine Vielzahl von Fluiden in einem weiten Betriebsbereich gut überein. Ein vereinfachtes Berechnungsverfahren wird vorgeschlagen.

ИССЛЕДОВАНИЕ ТЕПЛООБМЕНА ПРИ КОНДЕНСАЦИИ В СТРАТИФИЦИРОВАННОМ ДВУХФАЗНОМ ПОТОКЕ В ГОРИЗОНТАЛЬНЫХ ТРУБАХ

Аннотация—Исследуется теплообмен при конденсации в стратифицированном двухфазном потоке пара и жидкости в горизонтальных трубах. При анализе учитывается влияние межфазного взаимодействия, аксиального градиента давления, величины температуры насыщения, разности температур и эволюции стратификации, связанной с накапливанием слоя конденсата на нижней стенке трубы. Влияние этих параметров оценивается по отношению к характеристикам теплообмена периферийной пленки конденсата для условий паро-водяного ламинарного потока. Разработан теоретический метод расчета коэффициента теплообмена вдоль трубы. Получено хорошее соответствие теоретических расчетов с имеющимися в литературе экспериментальными данными для целого ряда жидкостей в относительно большом диапазоне рабочих условий. Предлагается простое корреляционное соотношение для коэффициента теплообмена, полученное на основе численного решения с помощью регрессивного анализа.